# ANALYSIS OF VIBRATION CHARACTERISTICS FOR RUBBING MACHINE BASED ON MODAL TEST

/

# 基于模态试验的揉碎机振动特性分析

**Yao YUE, Haiqing TIAN*, Fei LIU, Tao ZHANG, Dapeng LI, Di WANG**
College of Mechanical and Electrical Engineering, Inner Mongolia Agricultural University, Hohhot, China
*Tel：+86 18347980829；E-mail: hqtian@126.com*
*DOI: https://doi.org/10.35633/inmateh-68-04*

***Keywords:*** *rubbing machine, mechanical vibration, no load test, modal test, whole machine*

**ABSTRACT**

*Aiming at the problems of large vibrations and noise of a working stalk rubbing machine, this paper took the 9R-60 rubbing machine as the research object and used the B&K modal test system and the vibration test system to analyse the modal and no-load conditions of the whole machine. Through analysing modal test data, it was concluded that the first five natural frequencies of the machine were 95.262 Hz, 144.386 Hz, 288.198 Hz, 313.719 Hz and 326.140 Hz. The results showed that spindle rotation had a more significant effect on the vibration than the feed chain rotation; the maximum vibration acceleration occurred at the small motor frame at a spindle speed of 1700 r·min$^{-1}$ and a feed chain speed of 0.65 m·s$^{-1}$, which was 135.539 m·s$^{-2}$. The distribution of the amplitude statistical characteristics of the vibration signals follows the normal distribution and belongs to the stationary random process. The vibration was a self-excited vibration of the rotating machinery caused by the rotation of the main shaft and a forced vibration excited by the rotation of the same shaft. The research provides a direction for further research on the vibration characteristics of the rubbing machine under load conditions, and provides a theoretical basis for the subsequent vibration reduction design.*

**摘要**

*针对工作状态下揉碎机振动大、噪声大的问题，以 9R-60 揉碎机为研究对象，采用 B&K 模态测试系统与振动测试系统对其模态与空载工况进行分析。通过对模态试验数据的分析，得出其前五阶固有频率分别为 95.262 Hz、144.386 Hz、288.198 Hz、313.719 Hz 和 326.140 Hz。结果表明，主轴转动相比于喂入链转动对揉碎机振动的影响更为明显；在主轴转速 1700 r·min$^{-1}$、喂入链转速 0.65 m·s$^{-1}$ 时，小电机机架振动加速度最大，为 135.539 m·s$^{-2}$。振动信号的幅度统计特性分布服从正态分布，属于平稳随机过程。振动是由主轴旋转引起的旋转机械的自激振动和同轴旋转激发的强迫振动。该研究为进一步研究摩擦机在载荷条件下的振动特性提供了方向，并为后续的减振设计提供了理论依据。*

## INTRODUCTION

As one of the three main grains in China, maize is produced in considerable amounts annually. After harvest, a large number of stalks, which are rich in nutrients, remains. Stalks are an ideal source of feed. In the process of stalk forage, the stalk rubbing machine plays an important role. The rubbing machine can rub maize stalks into filaments, which are closer to the fodder, and have better palatability for cattle and sheep, which is beneficial to the feeding of ruminant livestock. However, the stalk rubbing machine currently on the market generally has problems with large vibrations and high noise, which restricts the popularization and use of the rubbing machine. At the same time, the vibration and noise generated in the feed production process not only pollute the environment but also cause physical and mental harm to workers (*Chen, 2020; Dobie et al., 2008; Li, 2017*). In addition, long-term vibration of the machine causes fatigue damage to the vibrating parts, loosening of screws and other problems (*Lu, 2019*).

Currently, many domestic and foreign studies on the vibration of rubbing machines mainly focus on the vibration characteristics of the main components and parts (*Wang et al., 2018; Lan et al., 2020*), the structure design and test of the machine (*Kakitis et al., 2016*), the modal simulation analysis and the vibration test (*Wang et al., 2010; Yan, 2018*), and suggestions for improvement are put forward based on the test and simulation results. In terms of vibration reduction of other agricultural machinery, domestic scholars have conducted research on the direction of vibration reduction through methods such as vibration tests (*Gao et al., 2017; Zhu et al., 2018; Xu et al., 2014*), modal tests (*Yao et al., 2017; Yao et al., 2018; Zhang et al., 2018*) and modal simulations (*Zhu et al., 2014; Yao et al., 2016; Sun et al., 2014*), and proposed vibration reduction directions such as resonance and dynamic balance. Among foreign

researchers, Tanas et al. obtained the natural frequency and damping parameters of a grain crusher machine through modal tests and combined these parameters to optimize the structure dynamics, thereby reducing the noise value of the whole machine (*Tanas et al., 2018*); Evandro P. da Silva and others carried out modal simulation of a coffee harvester in the empty state and full state and obtained its 20th-order modal frequency. Combined with the stress and displacement simulation results, it was concluded that the main motor of the coffee harvester may cause the fracture of the vibrating parts (*Evandro et al., 2018*). Hoshyarmanesh et al. used experiments and simulations of olive trees to obtain the natural frequency and other related parameters to obtain the best operating parameters, thereby improving productivity (*Hoshyarmanesh, et al., 2017*). This research conducted modal research and experimental exploration from the perspective of the research object, analysed vibration phenomena from multiple angles and used them to provide ideas and theoretical support for subsequent research.

Currently, there are few studies on the vibration of rubbing machines, and the existing research is mostly limited to earlier types of research. Modal test research on large-scale livestock machinery such as rubbing machines is mostly focused on key parts, but modal test research on the whole machine is limited. It is not easy to analyse the response after the system as a whole is subjected to excitation during operation. Based on these results, this paper took the 9R-60- type rubbing machine as an example, carried out a modal test to explore it, and obtained the first five natural frequencies of the whole rubbing machine. Furthermore, vibration tests under no-load conditions were carried out, and the vibrations under different speeds of the spindle and feed chain were analysed by using time domain and frequency domain analysis methods. Combined with the results of the modal test, the vibration characteristics of the rubbing machine under different excitations were obtained.

## MATERIALS AND METHODS

### Method principle analysis

In physical coordinates, a set of coupled second-order ordinary differential equations is often used to describe the motion of a multi-degree-of-freedom linear vibration system. The physical coordinates are transformed into modal coordinates by using the vibration mode matrix; the ordinary differential equation can be transformed into a set of mutually independent motion equations, each of which has the same structure as a single degree-of-freedom vibration system. This analysis method is called modal analysis.

In modal coordinates, modal parameters (natural frequency, mode shape, modal stiffness, etc.) are usually used to describe the dynamic characteristics of the system. The modal parameters of the system can generally be obtained by analytical calculations or dynamic testing methods.

The differential equation of motion of a damped system with multiple degrees of freedom is then

$$[M]\{\ddot{x}\} + [C]\{\dot{x}\} + [K]\{x\} = \{f\} \quad (1)$$

In the formula, [M] is the mass matrix, [C] is the damping matrix, [K] is the stiffness matrix, {x} is the response vector, and {f} is the force vector.

Under the action of an external force, the motion equation in the form of the state vector of the system is:

$$\begin{bmatrix} C & M \\ M & 0 \end{bmatrix} \begin{Bmatrix} \dot{x} \\ \ddot{x} \end{Bmatrix} + \begin{bmatrix} K & 0 \\ 0 & -M \end{bmatrix} \begin{Bmatrix} x \\ \dot{x} \end{Bmatrix} = \begin{Bmatrix} f \\ 0 \end{Bmatrix} \quad (2)$$

It is assumed that the external force acting on the system is simple and harmonic, that is,

$$\{f\} = \{F\}e^{i\omega t} \quad (3)$$

Then, the response of the physical coordinates and modal coordinates of the system is also simple and harmonic, namely,

$$\{x\} = \{X\}\, e^{i\omega t} \quad (4)$$

$$a_i = \begin{bmatrix} C & M \\ M & 0 \end{bmatrix} e^{i\omega t} \quad (5)$$

Where $a_i = \begin{Bmatrix} \Psi_i \\ s_i\Psi_i \end{Bmatrix}^T \begin{bmatrix} C & M \\ M & 0 \end{bmatrix} \begin{Bmatrix} \Psi_i \\ s_i\Psi_i \end{Bmatrix}$.

The matrix expression of the frequency response function of the multi-degree-of-freedom damped system is derived by the state space method as

$$[H(\omega)] = \sum_{i-1}^{n} \left( \frac{1}{a_i} \frac{\{\Psi_i\}\{\Psi_i\}^T}{i\omega - s_i} + \frac{1}{a_i^*} \frac{\{\Psi_i^*\}\{\Psi_i^*\}^T}{i\omega - s_i^*} \right) \quad (6)$$

Then, the complex frequency is $s_i = -\frac{a_i}{b_i}, b_i = \begin{Bmatrix} \Psi_i \\ s_i\Psi_i \end{Bmatrix}^T \begin{bmatrix} K & 0 \\ 0 & -M \end{bmatrix} \begin{Bmatrix} \Psi_i \\ s_i\Psi_i \end{Bmatrix}$; $\{\Psi_i\}$ is a complex modal vector.

In addition, the relevant theories of the modal assurance criterion (MAC) are also used. The MAC

matrix is the dot product of the vibration mode vectors and is a tool for evaluating the spatial correlation of the modal vectors. Its calculated variable values are between 0 and 1. Its expression is

$$\mathrm{MAC_{ij}} = \frac{(\phi_i^T \phi_j)^2}{(\phi_i^T \phi_i)(\phi_j^T \phi_j)} \quad (7)$$

Where $\phi_i$ and $\phi_j$ are the i-th-and j-th-order vectors of the vibration mode matrix, respectively.

If $\phi_i$ and $\phi_j$ are estimates of the same vibration mode by the same parameter identification method, i=j. The two modal vectors can be converted to each other according to a certain scale factor, so the values should be close in theory; therefore, the value of the ratio $\mathrm{MAC_{ij}}$ should be close to 1. If different vibration modes are estimated, theoretically, the value is relatively low, and the ratio $\mathrm{MAC_{ij}}$ value should be close to 0.

**Modal test**

The rubbing machine test bench is composed of a frame, throwing port, spindle rotor, feed inlet, and tooth plates, as shown in Fig. 1. The spindle rotor is located in the rubbing cavity, including the cutter structure, hammers, hammer rack and throwing mechanism; the rubbing chamber, frame, feeding part and throwing port are welded and fixed.

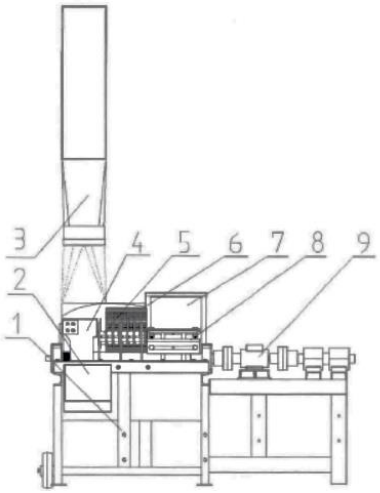


**Fig. 1 - Structure diagram of rubbing machine test bench**

*1. Frame; 2. Lower throwing port; 3. Upper throwing port; 4. Throwing mechanism; 5. Hammer; 6. Tooth plate; 7. Feeding inlet; 8. Cutter structure; 9. Spindle*

Due to the large mass and volume of the rubbing machine, the modal test was carried out by adding air spring cushions under the support feet of the machine. The cushion is an elastic element composed of an air chamber, a rubber elastic diaphragm, and a support plate. It is a flexible sealed container with compressed air, which provides resilience and support force by the restoring force of compressed air. As shown in Fig. 2(a), the model chosen is ALJ-51006 of An Lijing ® Company. The five supporting points were arranged on the cushions. At the same time, to make the rubbing machine as free as possible, a rubber pad was added between the machine and the cushions, as shown in Fig. 2(b). During the test, the height of each air spring cushion was measured, an air compression pump was used to inflate the cushions and ensure that each of the cushions had the same height change after inflation, which was 10 mm.

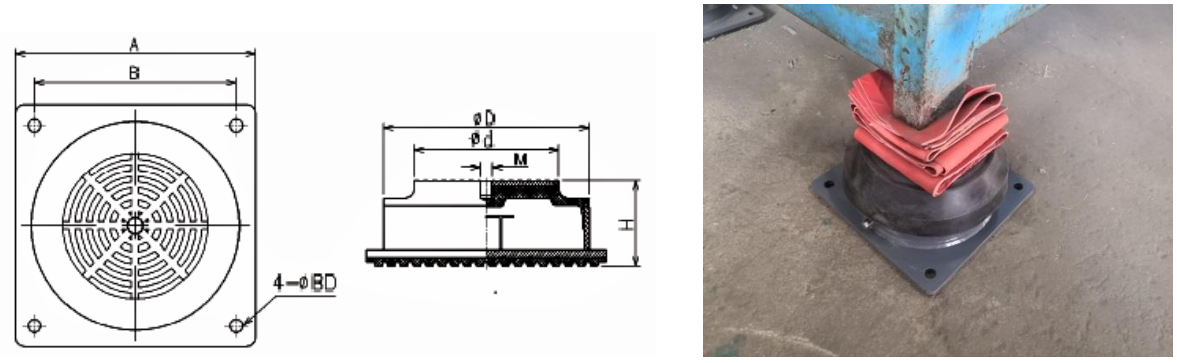


*a* *b*

**Fig. 2 - Structure and working diagram of air spring cushion**

To obtain the vibration characteristics of the machine, a force hammer was used to excite the structure. In the pre-tests, better results were obtained when aluminium hammer was used. Therefore, the modal test used an aluminium one.

The test used equipment from the Danish Company B&K, and the MTC Hammer module in the B&K's PULSE 16.0 software was used to collect and analyse data. The relevant models of the test equipment are shown in Tab. 1.

**Test Instruments** **Table 1**

| Instrument | Type |
|---|---|
| Aluminium hammer | 8206-002 |
| Triaxial acceleration sensor | 4507Bxyz |
| Data acquisition instrument | 3050-B-060 |
| Data acquisition software | PULSE 16.0 |
| Data post-processing module | Reflex |

The test used the single-input single-output method to process the input and output analogue signals through the data acquisition instrument. Here, the input signal was the excitation signal generated by using the roving hammer to knock the measuring points at different positions of the machine, and the output signal was collected by the three-axis acceleration sensor arranged at the fixed point. The data acquisition instrument and PULSE operation software sampled the analogue signal collected by the sensor at a certain time interval, namely discretization was performed. Then, each instantaneous analogue quantity of the discrete-time signal was converted into a digital quantity by an A/D conversion device, that is digitizing the signal, and finally the discrete-time digital signal was obtained. PULSE converted the received time domain digital signal to the frequency domain by FFT and other methods to obtain the frequency response function. The modal parameters of the structure were obtained by the modal parameter estimation algorithm.

Before the test, the data acquisition instrument was connected to the computer through a network cable, and the force hammer and the triaxial acceleration sensor were connected to the acquisition card to complete the hardware connection of the mould test system.

The model used in the test was a three-dimensional wireframe drawing, which compared to its outline is more conducive to analysing data and modal formation in the modal test. Since the test adopted a single reference measurement method and used a roving hammer to excite each measurement point, the theoretical vibration mode was analysed and calculated by finite element software before the reference point was selected, and the position of the node was observed. When placing the sensor, to avoid the modal nodes, select the main connection points, centre points, and boundary points of each part to mark and tap. A total of 48 points were selected for tapping with the hammer icon, as shown in Fig. 3. At the hitting point, the sensor was selected at a connection point on the rack, which is labelled 1 in the figure. The triaxial acceleration sensor was fixed, and the hammer was moved to strike each measuring point to complete the modal test.

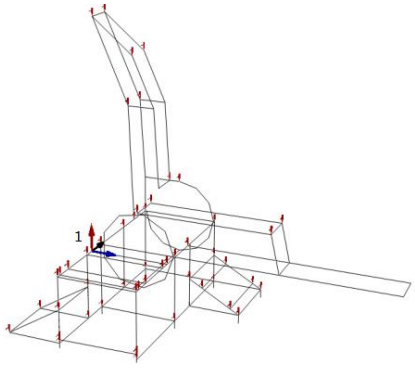


**Fig. 3 - Diagram of test points**

To ensure that the signal was not distorted after acquisition, the appropriate sampling frequency should be selected before the signal acquisition. Combined with the pre-tests and the working conditions, the sampling frequency was selected as 400 Hz, Lines was set as 400 Hz, and Span was 400 Hz, and Linear was selected as the average method. After the above arrangement and setting, each measuring point was tapped three times in the direction of the plumb weight. Throughout the calculation, a total of 144 taps were made.

**Vibration test**

After the modal test, the vibration under no load condition was studied. The vibration test instrument used the PULSE system and sensors produced by B&K. One triaxial acceleration sensor and three uniaxial acceleration sensors were arranged on the system to collect vibration data; the data collector received the data collected by the sensor. After analogue-to-digital conversion, it was transferred to the analysis and processing software; PULSE data acquisition analysis and processing software was used for parameter setting during the test process, online signal acquisition, and spectrum analysis of the collected data. The specific parameters of the equipment are shown in Tab. 2.

**Equipment parameter table** **Table 2**

| Instrument | Accuracy | Range |
|---|---|---|
| 4506-B triaxial acceleration sensor | 10mV/m·s-2 | 700 m·s-2<br>0.3-3.5k in X,Y and Z directions |
| 4507 single axial acceleration sensor | 10mV/m·s-2 | 700 m·s-2<br>0.3-6k in each directions |
| LAN-XI data acquisition front end | | |
| PULSE software | | |

To fully reflect the overall vibration as much as possible, the three-axis sensor was arranged on the outer sidewall of the machine, namely channels 1, 2, and 3. Channels 1-3 represent the z-direction, x-direction and y-direction where the machine was placed in the Cartesian coordinate system at the angle shown in Fig. 4. The other three single-axis acceleration sensors were arranged above the feed inlet, the small motor frame and the upper part of the rack, which were, channels 4, 5, and 6, as shown in Fig. 4. The uniaxial acceleration sensor and the triaxial acceleration sensor were connected to the data acquisition instrument, and the corresponding channel number was recorded.

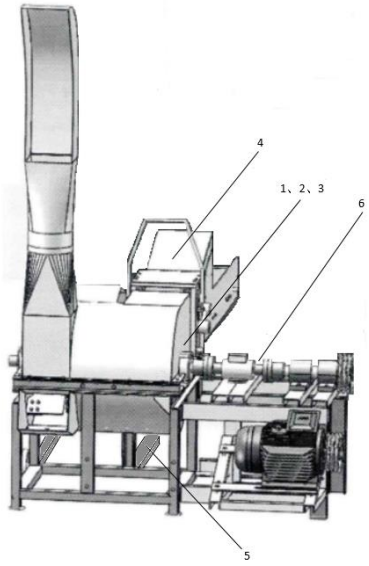


**Fig. 4 - Diagram of sensor layout**

Before testing, the parameters of the test system were set in the Labshop module of PULSE software. After the setting was completed, the no-load vibration test could be carried out. Referring to the general rules for the design of the rubbing machine rotor in the "Agricultural Machinery Design Manual" and the rotor specifications of this test system, the spindle speed was set to be 1200-1800 r·min$^{-1}$ during the test, and the interval was 100 r·min$^{-1}$, for a total of 7 groups . The feed chain speed referred to the productivity and other requirements in NY/T509-2015 "Technical Specification of Quality Evaluation for crop Straw rubbing filament Machines", set in the range of 0.35-0.65 m·s$^{-1}$, with an interval of 0.05 m·s$^{-1}$, a total of 7 groups. The vibration of the system was tested when the main shaft and the feed chain worked separately and when the two motors drove the main shaft rotor and the feed chain to rotate. Through analysis of single factor test results, it was concluded that when the spindle speed was 1600 r·min$^{-1}$ and the feed chain speed was 0.65 m·s$^{-1}$, the

frequency of the occurrence of vibration amplitude was higher than for other speeds. Therefore, under the condition of the two motors working separately, when the spindle speed changes, the feed chain speed was set to a fixed value, here 0.65 m·s$^{-1}$; when the feeding chain speed changed, it would be set to a new fixed value, here 1600 r·min-1. The spindle speed change values were selected as 1400 r·min$^{-1}$, 1500 r·min$^{-1}$, 1600 r·min$^{-1}$, 1700 r·min$^{-1}$ and 1800 r·min$^{-1}$, and the feed chain speed changed values for 0.45 m·s$^{-1}$, 0.50 m·s$^{-1}$, 0.55 m·s$^{-1}$, 0.60 m·s$^{-1}$and 0.65 m·s$^{-1}$, then 9 sets of tests were performed. In this test, the rubbing machine was placed on the softer soil.

## RESULTS

### Modal test results

The signal collected after exciting the measuring point was processed by the PULSE Reflex module in PULSE, and the frequency response function diagram is shown in Fig. 5.

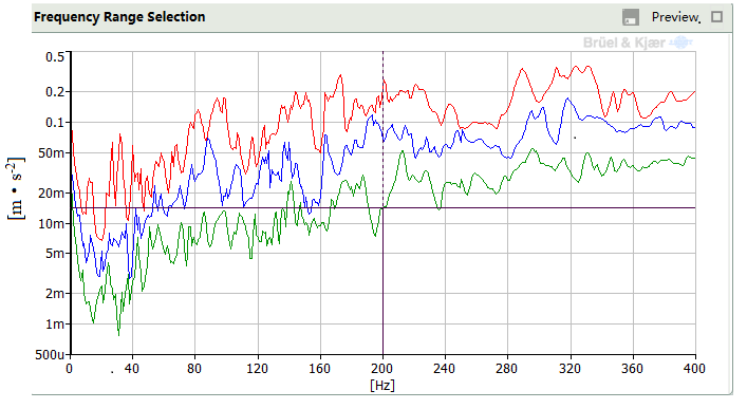


**Fig. 5 - Frequency response function**

The frequency response function was analysed, and only 40-360 Hz of the test frequency band 0-400 Hz was selected for data analysis to extract modal frequency bands of each order. The test results are shown in Tab. 3.

**First 5 natural frequencies** **Table 3**

| Order | Frequency /Hz | Damping /% |
|---|---|---|
| 1 | 95.262 | 3.154 |
| 2 | 144.386 | 2.483 |
| 3 | 288.198 | 1.899 |
| 4 | 313.719 | 0.851 |
| 5 | 326.140 | 2.521 |

### Vibration test results

After the vibration test, statistical parameters were used to describe the time domain results of this vibration test. The statistical results of the maximum vibration acceleration in the time domain data obtained in the single factor test are shown in Tab. 4.

**Statistical results of time domain maximum of single factor test** **Table 4**

| Test number | Spindle speed / r·min$^{-1}$ | Feed chain speed / m·s$^{-1}$ | Channel 1 / m·s$^{-2}$ | Channel 2 / m·s$^{-2}$ | Channel 3 / m·s$^{-2}$ | Channel 4 / m·s$^{-2}$ | Channel 5 / m·s$^{-2}$ | Channel 6 / m·s$^{-2}$ |
|---|---|---|---|---|---|---|---|---|
| 1 | 1200 | 0 | 23.851 | 78.602 | 27.336 | -24.409 | 21.574 | 21.574 |
| 2 | 1300 | 0 | -20.88 | -62.516 | -22.475 | -29.443 | 79.971 | 19.723 |
| 3 | 1400 | 0 | -27.587 | 75.221 | -23.082 | 25.81 | -116.811 | 22.55 |
| 4 | 1500 | 0 | -25.011 | -86.79 | -31.289 | -39.398 | -99.567 | -26.439 |
| 5 | 1600 | 0 | 32.412 | -96.549 | -34.579 | 36.393 | -123.116 | 31.627 |
| 6 | 1700 | 0 | -30.761 | 94.271 | 35.942 | 53.027 | 120.495 | 36.63 |
| 7 | 1800 | 0 | 30.002 | 92.155 | -27.344 | -43.764 | 121.135 | 38.489 |
| 8 | 0 | 0.35 | 9.014 | -28.494 | 11.809 | 22.392 | 36.733 | -3.89 |
| 9 | 0 | 0.4 | 18.85 | 42.342 | 12.972 | -21.782 | 26.615 | -3.406 |
| 10 | 0 | 0.45 | -10.378 | 41.784 | -13.411 | -18.082 | 35.128 | 5.056 |
| 11 | 0 | 0.5 | 10.533 | 36.888 | -12.17 | 20.776 | 35.75 | 4.419 |

| Test number | Spindle speed / r·min$^{-1}$ | Feed chain speed / m·s$^{-1}$ | Channel 1 / m·s$^{-2}$ | Channel 2 / m·s$^{-2}$ | Channel 3 / m·s$^{-2}$ | Channel 4 / m·s$^{-2}$ | Channel 5 / m·s$^{-2}$ | Channel 6 / m·s$^{-2}$ |
|---|---|---|---|---|---|---|---|---|
| 12 | 0 | 0.55 | -11.381 | -32.805 | -13.059 | 21.417 | 35.864 | 4.298 |
| 13 | 0 | 0.6 | 9.42 | -45.715 | -15.354 | 24.382 | -41.672 | -4.965 |
| 14 | 0 | 0.65 | -10.389 | -41.186 | -14.786 | -28.905 | 44.724 | 5.109 |
| 15 | 1600 | 0.45 | 23.533 | 102.668 | -35.177 | 41.628 | 109.148 | -32.37 |
| 16 | 1600 | 0.5 | 26.434 | 111.687 | 41.484 | 37.658 | 117.004 | 37.259 |
| 17 | 1600 | 0.55 | -28.548 | 79.407 | 33.541 | -44.993 | -104.56 | 37.306 |
| 18 | 1600 | 0.6 | -28.901 | -89.006 | 38.5 | 46.305 | -107.899 | 31.49 |
| 19 | 1600 | 0.65 | -31.946 | 86.377 | 29.376 | 40.35 | 113.535 | 32.008 |
| 20 | 1400 | 0.65 | -33.875 | 87.619 | 28.401 | 50.823 | 108.875 | -28.539 |
| 21 | 1500 | 0.65 | 30.836 | -74.062 | -30.025 | -44.825 | 116.421 | -30.548 |
| 22 | 1700 | 0.65 | -35.942 | -90.691 | -30.159 | -53.123 | 135.539 | 40.101 |
| 23 | 1800 | 0.65 | 38.483 | -104.983 | 37.778 | 29.902 | 122.071 | 35.296 |

Fig. 6(a) of the stacking histogram shows the amplitude of the corresponding frequency of each measuring point under 23 working conditions. And the distribution of amplitude is shown in Fig. 6 (b).

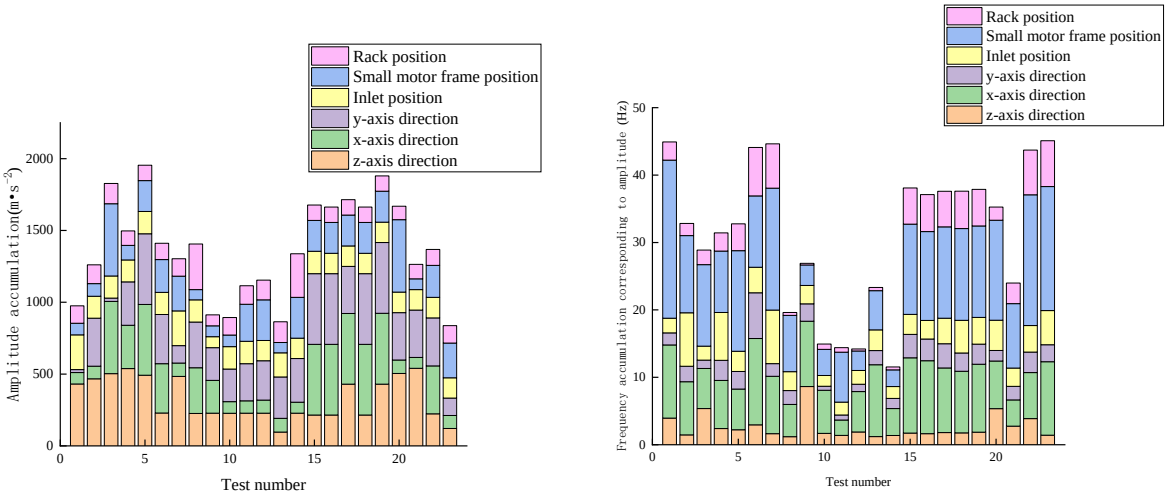


*a* *b*

**Fig. 6 - Frequency domain results stacking histogram**

## Discussion

The correlation of the model was analysed and its MAC matrix was obtained (*Yao et al., 2017; Su et al., 2021; Sayahkarajy et al., 2018*). It can be seen from Fig. 7 that the MAC value on the main diagonal element of the matrix is equal to 1, while the values outside the element were much less than 1. The MAC value of the same mode shape was 1, indicating that the theoretical mode shapes were correlated; for the smaller values, other than the non-diagonal elements of the matrix, it indicated that the calculated modes of each order were more independent, and the correlation was small, indicating that the test was more effective in extracting the modal parameters of the structure, and the test results had high credibility.

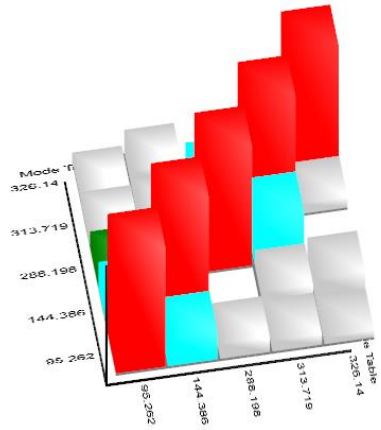


**Fig. 7 - MAC matrix chart**

By analysing and processing the time domain signal (*Liao et al., 2021*), the result is shown in Fig. 8.

It can be seen from Fig. 8 (a) that the vibration acceleration at each measuring point of the machine when only the spindle rotated (Test No. 1-7) is significantly higher than that when only the feeding chain worked (Test No. 8-14). The results show that the maximum vibration acceleration of the machine is -123.166 m·s$^{-2}$ and the minimum is 19.723 m·s$^{-2}$ when only the spindle rotates. The maximum vibration acceleration is -45.715 m·s$^{-2}$ and the minimum is -3.89 m·s$^{-2}$ when only the feeding chain rotates. It can be seen from Fig.8 (b) that with the increasing spindle speed, the vibration acceleration basically presents a trend of first increasing and then decreasing. It can be seen from Fig. 8 (c) that when two motors work at the same time (Test No. 15-23), the difference between the vibration acceleration value of the rubbing machine and the value when only the spindle rotates is small. Therefore, the influence of the feeding chain rotation on the vibration is less than that of spindle rotation, and spindle rotation is the main vibration cause of the vibration. It can be seen from Fig. 8 (d) that the maximum vibration acceleration (135.539 m·s$^{-2}$) occurs at the small motor frame under the condition of spindle speed 1700 r·min$^{-1}$ and feeding chain speed 0.65 m·s$^{-1}$. On the one hand, the mass of the small motor is larger, on the other hand, the cantilever of the motor frame is fixed on the frame, and the bottom does not contact the ground and other supports, which makes the external force have a longer action torque, so the vibration acceleration at this point is larger than that at other points, and the fatigue and other damage caused by vibration are relatively large.

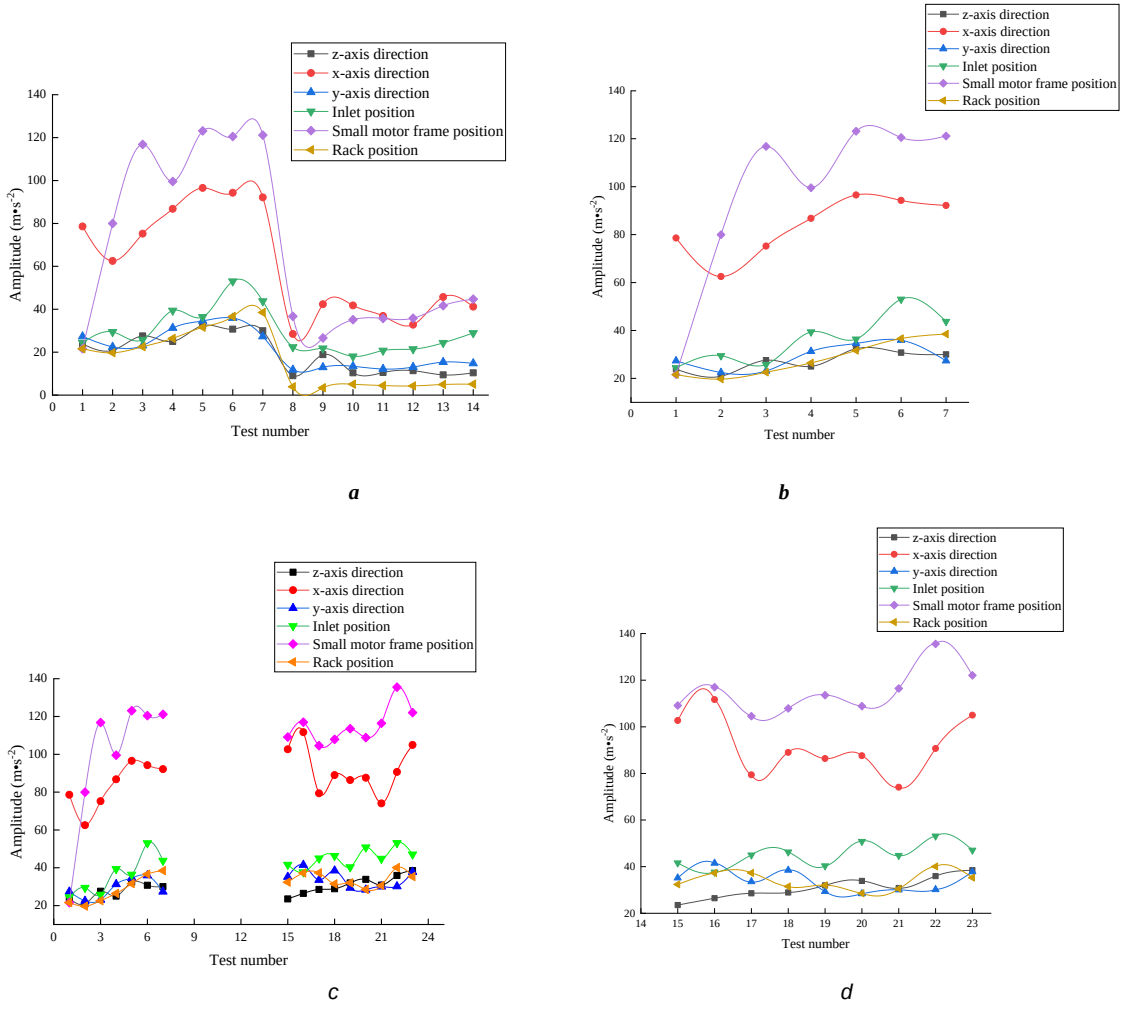


**Fig. 8 - Time domain amplitude analysis diagram**

By analysing the vibration acceleration data collected from the first three channels, we can get that, as far as the point on the wall of the rubbing chamber is concerned, when the spindle rotates and the feed chain rotates, the vibration of the left and right direction of the machine is obviously stronger than that of the front and rear directions and the up and down directions.

According to the frequency domain results (*Yao et al., 2015*), the range of amplitude frequencies is shown in Fig. 9(a). The frequencies corresponding to the amplitude fall in the centre of the range, which are 125 Hz, 225 Hz, 325 Hz and 75 Hz, account for approximately 0.681% of the total statistical data.

Combined with the results of the modal test, the natural frequencies are 95.262 Hz, 144.368 Hz and 313.719 Hz, which fall in the histogram of 75 Hz, 125 Hz and 325 Hz. It can be inferred that one of the reasons for the vibration of the rubbing machine is the self-excited vibration caused by the rotation of the main shaft. The frequency corresponding to the other amplitudes is 4-21 times the spindle speed frequency under the corresponding working conditions. It can be concluded that spindle rotation is the main cause of forced vibration.

It can be seen from the analysis in Fig. 9(b) that the random vibration signal obeys the Gaussian normal distribution, which is the expected curve form. Therefore, the distribution of the amplitude statistical characteristics of the vibration signals of the six measuring points of the machine approximately obeys the normal distribution, and it can be considered that the vibration under each no-load condition belongs to a stationary random process.

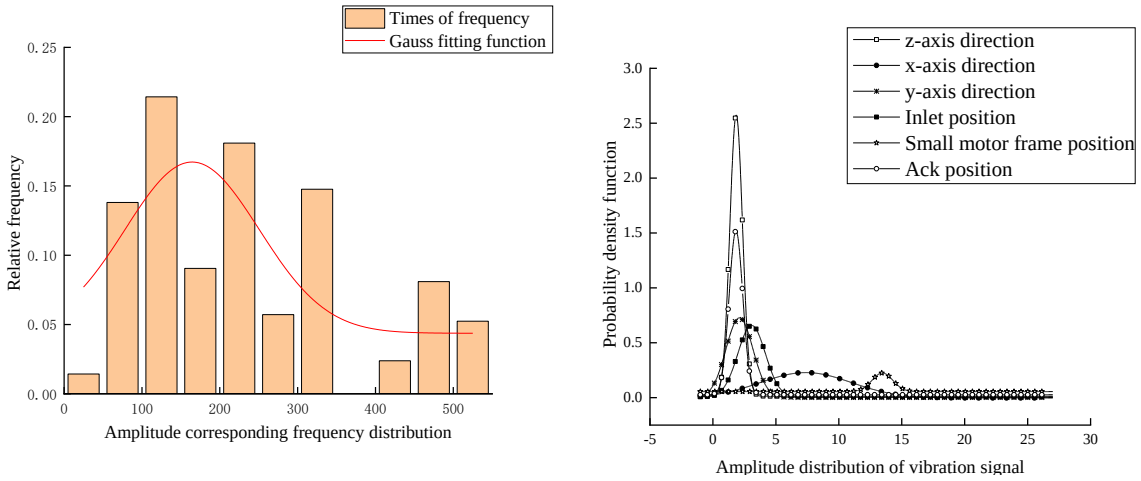


*a* *b*

**Fig. 9 - Distribution diagram**

**ACKNOWLEDGMENT**

The supports of the National Natural Science Foundation of China (NSFC) (No. 51905277) and the Inner Mongolia Special Project for Transformation of Scientific and Technological Achievement (No. 2019CG034), National Natural Science Foundation of China (No. 32071893) for this research are greatly appreciated.

**REFERENCES**

[1] Chen Q.S., (2020), Focus on prevention and control of noise and hand-arm vibration, and protect workers' health (*关注噪声和手传振动防控*). *Journal of Environmental and Occupational Medicine.* 37(04):334-336. doi: 10.13213/j.cnki.jeom.2020.20099;

[2] Dobie Robert A., (2008), The burdens of age-related and occupational noise-induced hearing loss in the United States. *Ear and Hearing*. 29(4):565-577. doi: 10.1097/AUD.0b013e31817349ec;

[3] Evandro P da Silva; Fábio M da Silva; Ednilton T de Andrade; Ricardo R Magalhães, (2018), Structural static and modal frequency simulations in a coffee harvester's chassis. *Revista brasileira de engenharia agricola e Ambiental.* 22(7): 511-515.

[4] Gao Z.P., Xu L.Z., Li Y.M., Wang Y.D., Sun P.P., (2017), Vibration measure and analysis of crawler-type rice and wheat combine harvester in field harvesting condition. (*履带式稻麦联合收获机田间收获工况下振动测试与分析*) *Transactions of the Chinese Society of Agricultural Engineering*. 33(20):48-55.

[5] Hoshyarmanesh H., Dastgerdi H.R., Ghodsi M., Khandan R., Zareinia K., (2017), Numerical and experimental vibration analysis of olive tree for optimal mechanized harvesting efficiency and productivity. *Computers and electronics in agriculture* 132: 34-48.

[6] Kakitis A., Berzins R., Berzins U., (2016), Cutting energy assessment of hemp straw. *Engineering for Rural Development*, Jelgava, (Latvia), May 25-27. pp: 1255-1259;

[7] Lan Y.Z.; Zhang L., Zhai Z.P., Li Z.W., Li C., (2020), Analysis of the Influences of Structure Parameters on Pneumatic Noise of the Impeller Blower of the Stalk Rubbing Machine. (*结构参数对秸秆揉碎机抛送装置气动噪声的影响分析*) *Journal of Agricultural Mechanization Research*. 42(12):34-38+63. doi: 10.13427/j.cnki.njyi.2020.12.006)

[8] Li T., (2017), Explore the Syrian Industrial Production Vibration Harm and Control Countermeasures. (*工业生产振动的危害及其控防对策研究*) *China Personal Protective Equipment* (02):48-52. doi: 10.16102/j.cnki.cppe.2017.02.011;

[9] Liao Y.T., Qi T.X., Liao Q.X., Zeng R., Li C.L., Gao L.P., (2021), Vibration characteristics of pneumatic rape precision combine direct seeder and its effect on seeding performance. (*气力式油菜精量联合直播机振动特性及对排种性能影响*) *Journal of Jilin University (Engineering and Technology Edition)*, doi: 10.13229/j.cnki.jdxbgxb20210001;

[10] Lu Y.H., (2019), Preface to the topic "study on fatigue in vibration environment". (*振动环境下疲劳问题研究"专题序言*). *Equipment Environmental Engineering.* 16(11):10+9;

[11] Sayahkarajy, M, (2018), Mode shape analysis, modal linearization, and control of an elastic two-link manipulator based on the normal modes. *Applied mathematical modelling* 59: 546-570. https://doi.org/10.1016/j.apm.2018.02.003;

[12] Su H.J., Cui H.M., Li F.Y., (2021), Free Modal Test and Analysis of Air Blown Deep Loose Shovel. (*气吹式深松铲自由模态试验与分析*). *Journal of Agricultural Mechanization Research.* 43(05):212-216+262.

[13] Sun Z.., Wang L., Pan Z.., (2014), Analyses of vibration characteristics of power fan for the 4ztl-1800 pneumatic conveying combine stripper harvester. *Transactions of the ASABE.* 57(3): 693-699.

[14] Tanas W., Szczepaniak J., Kromulski J., Szymanek M., Tanas J., Sprawka M., (2018), Modal analysis and acoustic noise characterization of a grain crusher. *Annals of agricultural and environmental medicine.* 25(3):433-436. Doi:10.26444/aaem/87154;

[15] Wang J.B., Dong H.J., Zhai Z.P., Cheng H.Y., Kang X.Y., Wu Y.M., (2018), Modal Analysis and Structure Optimization of the Rotors of Forage Rubbing and Breaking Machines. (*饲草揉碎机转子模态分析及结构优化*). *Noise and Vibration Control.* 38(05):52-56+61;

[16] Wang J., (2010), *Study on noise of 9R-40 rubbing and breaking machine. (9R-40 型揉碎机噪声分析研究)*. PhD thesis. Univ. Inner Mongolia agricultural, Hohhot, China;

[17] Xu L.Z., Li Y.M., Su P.P., Pang J., (2014), Vibration measurement and analysis of tracked-whole feeding rice combine harvester. (*履带式全喂入水稻联合收获机振动测试与分析*) *Transactions of the Chinese Society of Agricultural Engineering*. 30(08):49-55. doi:CNKI:SUN:NYGU.0.2014-08-006;

[18] Yan P., (2018), *Test research on the performance and vibration of the 9RS-60 stalk rubbing machine*. (*9RS-60 型揉碎机性能试验与振动测试研究*) MSc thesis. Univ. Inner Mongolia agricultural, Hohhot, China;

[19] Yao Y.C., Du Y.F., Zhu Z.X., Mao E.R., Song Z.H., (2015), Vibration characteristics analysis and optimization of corn combine harvester frame using modal analysis method. (*基于模态的玉米收获机车架振动特性分析与优化*). *Transactions of the Chinese Society of Agricultural Engineering.* 31(19):46-53.

[20] Yao Y.C., Song Z.H., Du Y.F., Mao E.R., Zhao X.Y., Zhang W.R., (2016), Optimum seeking of spot weld model on numerical simulation of stress and modal analysis for corn combine harvester frame. (*玉米收获机车架应力及模态数值模拟焊点模型优选*) *Transactions of the Chinese Society of Agricultural Engineering.* 32(24):50-58. doi:CNKI:SUN:NYGU.0.2016-24-007;

[21] Yao Y.C., Song Z.H., Du Y.F., Zhao X.Y., Mao E.R., Liu F., (2017), Analysis of vibration characteristics and its major influenced factors of header for corn combine harvesting machine. (*玉米收获机割台振动特性及其主要影响因素分析*) *Transactions of the Chinese Society of Agricultural Engineering.* 33(13):40-49;

[22] Yao Y.C., Zhao X.Y., Du Y.F., Song Z.H., Yin Y.Y., Mao E.R., Liu F., (2018), Operating modal analysis and test of harvester induced by mass-varying process. (*考虑质量时变的收获机械工作模态分析与试验*) *Transactions of the Chinese Society of Agricultural Engineering* 34(09): 83-94. doi:CNKI:SUN:NYGU.0.2018-09-010;

[23] Zhang J.X., Yang C., Zhang L., Jiang Y.X., Wang C.Y., (2018), Analysis and experiment on strength and vibration characteristics of corn stubble plucking mechanism. (*玉米起茬机构的强度及振动特性分析与试验*), *Transactions of the Chinese Society of Agricultural Engineering*. 34(12):72-78. doi:CNKI:SUN:NYGU.0.2018-12-009;

[24] Zhu L.H., Li Y.M., Tang Z., Xu L.Z., (2018), Vibration Test and Analysis of the All-in-one Machine of Combine Harvester and Baler. (*联合收获打捆复式作业机振动测试与分析*), *Journal of Agricultural Mechanization Research.* 40(03):146-151. doi:10.13427/j.cnki.njyi.2018.03.029;

[25] Zhu S.H., Xu G., Yuan J.Q., Ma J.F., Yi Lidaer Li K., (2014), Influence of implement's mass on vibration characteristics of tractor-implement system. (农具质量对拖拉机悬挂农具系统振动特性的影响), *Transactions of the Chinese Society of Agricultural Engineering.* 30(24):30-37. doi:CNKI:SUN:NYGU.0.2014-24-004.